

Deciphering the mechanism of potent peptidomimetic inhibitors targeting plasmepsins – biochemical and structural insights

Vandana Mishra¹, Ishan Rathore¹, Anagha Arekar¹, Lakshmi Kavitha Sthanam¹, Huogen Xiao², Yoshiaki Kiso³, Shamik Sen¹, Swati Patankar¹, Alla Gustchina⁴, Koushi Hidaka⁵, Alexander Wlodawer⁴, Rickey Y. Yada⁶ and Prasenjit Bhaumik¹

1 Department of Biosciences and Bioengineering, Indian Institute of Technology Bombay, Powai, Mumbai, India

2 Department of Molecular and Cellular Biology, University of Guelph, ON, Canada

3 Laboratory of Peptide Sciences, Nagahama Institute of Bio-Science and Technology, Japan

4 Protein Structure Section, Macromolecular Crystallography Laboratory, National Cancer Institute, Frederick, MD, USA

5 Division of Pharmaceutical Chemistry, Faculty of Pharmaceutical Sciences, Kobe Gakuin University, Japan

6 Faculty of Land and Food Systems, University of British Columbia, Vancouver, BC, Canada

Keywords

crystal structures; drug designing; KNI inhibitors; malaria; plasmepsins

Correspondence

P. Bhaumik, Department of Biosciences and Bioengineering, Indian Institute of Technology Bombay, Powai, Mumbai-400076, India

Fax: +91 22 25723480

Tel: +91 22 25767748

E-mail: pbhaumik@iitb.ac.in

Vandana Mishra and Ishan Rathore have contributed equally.

(Received 19 April 2018, revised 10 June 2018, accepted 22 June 2018)

doi:10.1111/febs.14598

Malaria is a deadly disease killing worldwide hundreds of thousands people each year and the responsible parasite has acquired resistance to the available drug combinations. The four vacuolar plasmepsins (PMs) in *Plasmodium falciparum* involved in hemoglobin (Hb) catabolism represent promising targets to combat drug resistance. High antimalarial activities can be achieved by developing a single drug that would simultaneously target all the vacuolar PMs. We have demonstrated for the first time the use of soluble recombinant plasmepsin II (PMII) for structure-guided drug discovery with KNI inhibitors. Compounds used in this study (KNI-10742, 10743, 10395, 10333, and 10343) exhibit nanomolar inhibition against PMII and are also effective in blocking the activities of PMI and PMIV with the low nanomolar K_i values. The high-resolution crystal structures of PMII–KNI inhibitor complexes reveal interesting features modulating their differential potency. Important individual characteristics of the inhibitors and their importance for potency have been established. The alkylamino analog, KNI-10743, shows intrinsic flexibility at the P2 position that potentiates its interactions with Asp132, Leu133, and Ser134. The phenylacetyl tripeptides, KNI-10333 and KNI-10343, accommodate different ρ -substituents at the P3 phenylacetyl ring that determine the orientation of the ring, thus creating novel hydrogen-bonding contacts. KNI-10743 and KNI-10333 possess significant antimalarial activity, block Hb degradation inside the food vacuole, and show no cytotoxicity on human cells; thus, they can be considered as promising candidates for further optimization. Based on our structural data, novel KNI derivatives with improved antimalarial activity could be designed for potential clinical use.

Database

Structural data are available in the PDB under the accession numbers 5YIE, 5YIB, 5YID, 5YIC, and 5YIA.

Abbreviations

Apns, allophenylnorstatine; Dmt, dimethylthioprolin; HAP, histo-aspartic protease; Hb, hemoglobin; Mta, methylthioalanine; PMII, plasmepsin II; PMI, plasmepsin I; PMIV, plasmepsin IV; PMs, plasmepsins.

Introduction

Malaria has been one of the most serious infectious diseases in the world. It spreads through transmission of the unicellular eukaryotic protozoans of the genus *Plasmodium*, with five known species (*Plasmodium falciparum*, *P. vivax*, *P. ovale*, *P. malariae*, and *P. knowlesi*) affecting humans. *Plasmodium falciparum* is the most virulent species and an obligate intracellular parasite, causing a majority of malaria deaths [1]. An estimated 212 million new cases of malaria and approximately 429 000 malaria deaths were recorded worldwide in 2015, especially among children [2]. The dangerous and unique pathogenesis of the parasite as well its ability to develop drug resistance augments the severity of the disease. The development of resistance in *P. falciparum* to all the currently used antimalarial drugs, including quinine, mefloquine, halofantrine, cycloguanil, sulfonamides, piperazine, and, recently, artemisinin along with its derivatives [3] has led to the increased global efforts toward discovery of novel and long-lasting drugs. Most of the existing antimalarial drugs act primarily at the erythrocytic stages of the life cycle of parasites, although the mechanism of action of many drugs is not fully understood [4]. This intraerythrocytic stage is crucial for the survival of the parasite that depends on consumption of host hemoglobin (Hb) inside the acidic food vacuole, providing the main source of amino acids for its growth and maturation [5,6]. Recent advances in understanding the pathophysiology of parasite have identified plasmepsins (PMs) as attractive drug targets [7]. All the PMs are pepsin-like aspartic proteases. Of the 10 different PMs encoded by the genome of *P. falciparum*, the four vacuolar PMs, PMI, II, IV, and the closely related histo-aspartic protease (HAP) participate actively in Hb catabolism [8,9].

The use of PMs as therapeutic targets presents several challenges to the drug development process. The reports based on the knockout studies [10,11] indicate that simultaneous inhibition of all these highly homologous (50–79% sequence identity) proteases is essential to kill the parasite owing to their functional redundancy. PMII shares 35% sequence identity with its closest human homolog, cathepsin D (Cat D), a pepsin-like enzyme. The active site regions of PMII and Cat D are even more identical, which suggests the need to design specific inhibitors that would avoid any cross-reaction with the human proteases. Along with the selectivity issues, the inadequate bioavailability of the designed inhibitors in the infected erythrocytes is also a major concern to be addressed. Despite several efforts toward drug development targeting PMs [12–16], only limited number of studies [17–20]

demonstrate the inhibition of multiple vacuolar PMs by a single inhibitor. Moreover, the difficulty in producing soluble recombinant PMs creates a roadblock for the high-throughput drug discovery against these crucial targets. So far, all the inhibition studies have been reported using the refolded PMs, and therefore, evaluating the inhibition of soluble PMs could be a better approach to designing novel drugs as well as to simplifying the process of antimalarial drug design.

Several crystal structures of PMII complexed with various inhibitors have been determined [21], which includes a total of 21 PMII structures in Protein Data Bank (PDB); however, if we consider the relevance of the structures in the context of drug development, there are only 10 PMII structures of the complexes with novel inhibitors. Furthermore, none of the available PMII structures represent any complex with the potent KNI inhibitors, distinctly different from all the other inhibitors for which the available PMII complexed structures are reported in PDB. Although only four structures of other vacuolar PMs (PMI, HAP, and PMIV) with the KNI inhibitors are known, these low-resolution structures with the inhibitors bound in the unusual orientation in the active sites of PMs provide only limited mechanistic insights. Therefore, detailed understanding of the binding and inhibition mechanism of the KNI inhibitors would be highly valuable toward rational designing of the novel compounds.

The KNI compounds were originally designed as inhibitors against HIV-1 protease and had also been recognized to target PMs. They are peptidomimetic inhibitors replacing the active site catalytic water molecule with the hydroxyl group of the allophenyl-norstatine moiety that resembles the reaction transition state [22]. In general, the KNI compounds have a common scaffold consisting of allophenyl-norstatine [(2S,3S)-3-amino-2-hydroxy-4-phenylbutyric acid] (Apns), a unique unnatural amino acid which is α -hydroxy- β -amino acid derivative, with a hydroxymethylcarbonyl isostere. This scaffold is designed on the basis of primary cleavage site of PMII, that is, the peptide bond between Phe33 and Leu34 in the α -chain of Hb [22]. While the Apns core is conserved, the outer parts of the molecule are held to its core by rotatable bonds which easily adapt to the variations in the binding sites of PMs, thus maintaining their potency toward all the four vacuolar PMs [23]. Some of these compounds have low toxicity and have the potential to be developed into effective antimalarial drugs [24–26]. One of the KNI inhibitors, KNI-10006, was found to inhibit the functions of vacuolar PMs with different binding affinity. The chemical structure

of KNI-10006 includes Apns at P1, 2,6-dimethylphenyloxyacetyl at P2, dimethylthioprolin (Dmt) at P1', and 2-aminoindanol at P2' site [17]. A few previously reported structures of PMs complexed with the KNI inhibitors [27–29] indicate that these compounds can adopt multiple conformations upon binding to PMs, depending on the arrangement and nature of the active site residues. Recently, the nonvacuolar PMs have been shown to be crucial for the viability of the parasites [30–33]. Interestingly, the KNI compounds were also successful in inhibiting the action of a nonvacuolar PM, PMV, another potential antimalarial drug target [34,35]. However, these reports did not shed any light on further development of these inhibitors as antimalarial drugs, primarily due to the lack of structural details to decipher the molecular basis of potency of the KNI compounds.

In this study, we prepared the soluble recombinant vacuolar PMs (PMI, PMII, HAP, and PMIV). We further evaluated the inhibition kinetics of PMI, PMII, and PMIV with different KNI compounds. Among the inhibitors used, KNI-10743 and KNI-10333 exhibited low nanomolar K_i values, showed considerable antimalarial activity, and displayed negligible cytotoxicity. Detailed crystal structures analysis of the PMII–KNI inhibitor complexes revealed the mechanism underlying the high inhibitory activities of the KNI compounds. Based on our biochemical and structural analysis, further modifications to KNI-10743 and KNI-10333 could increase their efficacy as potent inhibitors in targeting the PM family, thus suggesting a clear roadmap for improvement of these inhibitors as effective antimalarial drugs.

Results

Expression, purification, and activation of the vacuolar PMs

The expression, purification, and activation of soluble PMII were optimized first. For this purpose, the pET32b vector containing the truncated PMII (Lys77P–Leu329) zymogen, referred to here as tPMII, was expressed as a thioredoxin (Trx) tagged fusion protein (Trx-tPMII) in *Escherichia coli* Rosetta-gami B (DE3) pLysS cells (Fig. 1A). The purification of Trx-tPMII from the cell lysate supernatant was accomplished by using a combination of affinity and size exclusion chromatography. The eluted fractions containing Trx-tPMII from the Ni-NTA column were observed on SDS/PAGE at ~ 60 kDa, along with impurities (Fig. 1B). The SDS/PAGE of eluted fractions from the Superdex 75 16/600 shows the presence

of two purified forms, the fusion protein, Trx-tPMII (~ 60 kDa) and the truncated zymogen, tPMII at ~ 43 kDa (after cleavage of the tags; Fig. 1C). During purification, concentration, and storage of Trx-tPMII at 4 °C in phosphate buffer containing CHAPS detergent, we observed cleavage of the N-terminal tags that produced tPMII zymogen, thus omitting an additional protease-assisted cleavage process. The purified tPMII was activated to the ~ 37 kDa mature form [mature PMII (mPMII)] upon acidification, as observed by the band shift on SDS/PAGE (Fig. 1D).

The expression and purification of soluble fusion proteins, Trx-tPMI, Trx-tPMIV, and Trx-tHAP and their conversion into the zymogen forms were performed similarly as for PMII, with such procedures also leading to activation of purified PMI, HAP, and PMIV zymogens. The mature forms of PMI and PMIV with similar molecular weight (~ 37 kDa) were obtained in sufficient quantity and were used for inhibition studies. However, activation of HAP zymogen was very challenging, and thus, only a very small amount of the mature enzyme (~ 37 kDa) was obtained.

Enzyme activity and inhibition of PMII

Degradation of Hb by mPMII is evidenced by the smearing of bands at ~ 29 kDa and ~ 14 kDa (Fig. 2A). The direct indication of Hb degradation by PMII confirms the activity of the mature enzyme. The mature PMII cleaves the fluorogenic substrate with the K_m value of ~ 0.68 μM . Pepstatin A, a general inhibitor of pepsin-like aspartic proteases, strongly inhibits the mature enzyme with the K_i value of 0.07 nM. All the tested KNI compounds used in this study have been found to be highly potent against PMII with the K_i values in the low nanomolar range. KNI-10743 has significantly better inhibitory activity than KNI-10742, although they are structurally very similar. Despite similar structures of KNI-10395, KNI-10333, and KNI-10343, KNI-10333 possesses the highest inhibitory activity with a K_i value of 1.3 nM (Fig. 2B,C).

Quality of the PMII–KNI inhibitor complexed structures

In this study, we have determined the high-resolution crystal structures of PMII–KNI inhibitor complexes. Interestingly, all the crystal structures of PMII–KNI inhibitor complexes reported in the present study show opposite orientation of the inhibitors in the PMII active site when compared to the mode of binding of pepstatin A. However, orientation of the central

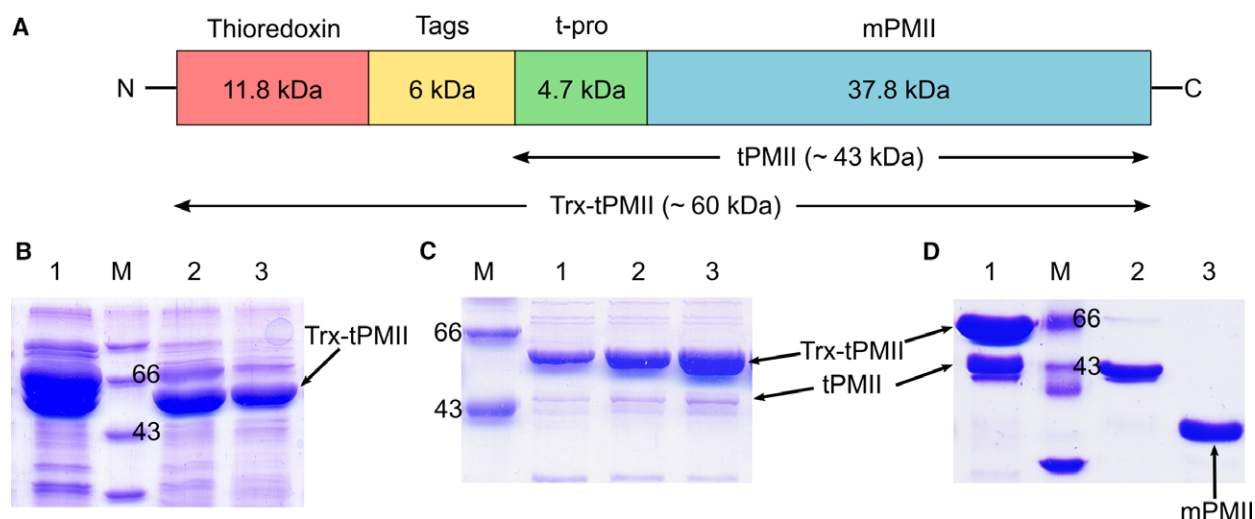


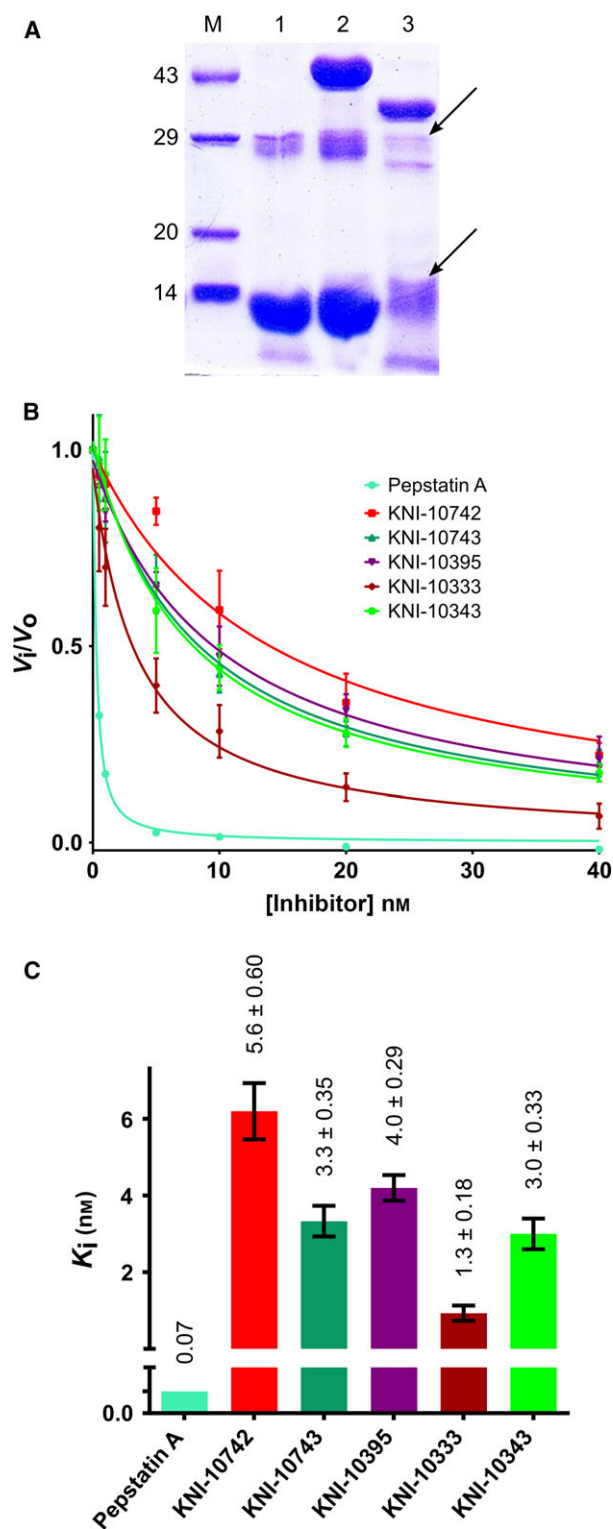
Fig. 1. Expression, purification, and activation of PMII zymogen. (A) Schematic diagram of the recombinant Trx-tPMII fusion protein consisting of Thioredoxin (Trx, 11.8 kDa), Tags (6 kDa including thrombin cleavage site, His-Tag, S-Tag, enterokinase cleavage site), and truncated PMII devoid of the first 76 amino residues (tPMII, Lys77P–Leu329, 42.5 kDa). The mPMII denotes the activated region after an autocatalytic cleavage at low pH. (B) The SDS/PAGE of fractions after a Ni-NTA affinity purification shown in lanes 1, 2, and 3 eluted at 75, 125, and 250 mM, imidazole concentrations, respectively. (C) SDS/PAGE showing the eluted fractions from the Superdex 75 16/600 column. Lanes 1–3: fractions eluted from 48 to 60 mL of column volume. The full length fusion protein, Trx-tPMII at ~60 kDa and truncated PMII zymogen, tPMII at ~43 kDa are labeled and marked by arrows. (D) SDS/PAGE showing tPMII zymogen before and after the activation. Lane 1: purified and pooled fraction of Trx-tPMII (~60 kDa) and tPMII (~43 kDa) zymogens after gel filtration, Lane 2: tPMII after the cleavage of N-terminal tags in the presence of phosphate buffer containing 0.15 M NaCl, and 0.2% CHAPS, pH 7.4, Lane 3: mPMII (denoted by arrow) at ~37 kDa upon acidification of tPMII in 0.1 M sodium acetate pH 4.5 at 37 °C for 4 h. The lane M in B, C, and D represents the protein molecular weight (kDa) marker.

hydroxyl groups is the same for both pepstatin A and the KNI inhibitors. This feature of the KNI compounds has also been seen in a few previously reported structures of the PM-inhibitor complexes [27–29]. Based on the substitutions at P2 and P3 positions in KNI-10006, we have classified these KNI inhibitors into two groups, the alkylamino analogs [Fig. 3A (i, ii)] and the phenylacetyl tripeptides [Fig. 3A (iii–v)]. As a result of the reverse orientation of the main chain of the KNI inhibitors in the active site of PMII as compared to the other peptidomimetic inhibitors bound to pepsin-like aspartic proteases, the P1 Apns group of the inhibitor is located in the S1' pocket and the P1' Dmt group is placed in the S1 pocket of the enzyme (Figs 4E and 5G; the assignment of the binding pockets follows the accepted nomenclature [36]).

The structures of the PMII–KNI inhibitor complexes presented in this study are of high quality, as quantified by the low *R*-factors and good stereochemical properties (Table 1). The unambiguous omit $F_o - F_c$ electron density clearly suggests the presence and orientation of the inhibitors in the active sites of all the complexed structures (Fig. 3B). The central hydroxyl groups of the inhibitors are placed between

the two catalytic aspartates (Asp36 and Asp216) of PMII. The flap is in the closed conformation in all the structures due to the binding of inhibitor. The hydrophobic CHAPS molecules are present on the surface of PMII–KNI inhibitor complexes and confer stability to the structures. All the main chain atoms and most of the side chains fit well into the $2F_o - F_c$ electron density maps. The quality of the final $2F_o - F_c$ electron density maps in the active sites is also optimal, defining the conformations of inhibitors in an unambiguous manner in all the complexed structures.

In the structures of pepsin-like aspartic proteases reported to date, the carboxylate groups of the two catalytic aspartates are coplanar [37]. Interestingly, there is a rotation in the plane of the carboxylate group of Asp216 with respect to the carboxylate group of Asp36 in all the PMII–KNI inhibitor complexes. This nonplanarity of aspartates is observed for the first time in any pepsin-like aspartic protease with bound inhibitor and might represent a crucial conformational state of the active site during catalysis. The nonplanar arrangement of the catalytic aspartates has been reported once previously, but in an uncomplexed structure of PMII [38].



In two complexed structures, PMII–KNI-10742 and PMII–KNI-10395, a sodium ion is located between the catalytic aspartates and the inhibitor (Figs 4A and

Fig. 2. Enzyme activity and inhibition of PMII. (A) SDS/PAGE showing the Hb degradation (marked with arrows at ~29 and ~14 kDa) by mPMII. Lane 1: human Hb control, Lane 2: Hb and tPMII mixture at 37 °C, Lane 3: Hb, mPMII, and sodium acetate buffer (0.1 M, pH 4.5) at 37 °C. Lane M represents the protein molecular weight (kDa) marker. (B) The inhibition kinetics of the various KNI compounds against PMII. (C) The bar graphs represent the K_i values of various KNI inhibitors and pepstatin A against PMII. The K_i values are labeled on the bar graph. The experiments are performed in triplicate ($n=3$) and the error bars represent \pm SEM.

5A). The presence of a tightly bound sodium ion in these PMII-inhibitor complexes might be due to the high concentration of sodium ions in the crystallization buffer that contains 1.4 M sodium citrate. The coordination geometry of the sodium ion in the active site and analysis with the CheckMyMetal server (https://csgid.org/metal_sites) confirmed the identity of the ion. However, no sodium ion is present in PMII–KNI-10743, PMII–KNI-10333, and PMII–KNI-10343 complexes, as these were crystallized in the conditions without any sodium salt.

Crystal structures of PMII complexed with KNI inhibitors containing alkylamino substituents (KNI-10742 and KNI-10743)

KNI-10742 and KNI-10743 belong to a group of inhibitors that have basic alkylamino chain at the 4-position of the phenyl group in the 2,6-dimethylphenoxyacetyl moiety [Fig. 3A (i,ii)]. KNI-10742 consists of a diethyl group and a slightly extended KNI-10743 has trimethyl substitutions in the alkylamino chain at the P2 position. In order to understand the structural basis of higher potency of KNI-10743 over KNI-10742 despite being structurally very similar, crystal structures of PMII in complexes with these inhibitors have been determined. The structures of the PMII–KNI-10742 and PMII–KNI-10743 complexes have been solved at 2.1 and 2.15 Å resolution, respectively. The data collection and refinement statistics for these structures are presented in Table 1. The omit $F_o - F_c$ maps of the bound inhibitors are shown [Fig. 3B (i,ii)]. Superposition of 327 C α atoms of both the complexed structures indicate that they are almost identical [root-mean-square deviation (r.m.s.d.) = 0.27 Å], with minor differences in orientation of the inhibitors at the P2 position.

The inhibitors are anchored in the active site of PMII through various hydrogen bonds and hydrophobic interactions (Fig. 4A–E). These interactions were also analyzed by LIGPLOT v.1.4.5 (Fig. 6A,B) [39]. The 2-aminoindanol moiety at the P2' position forms

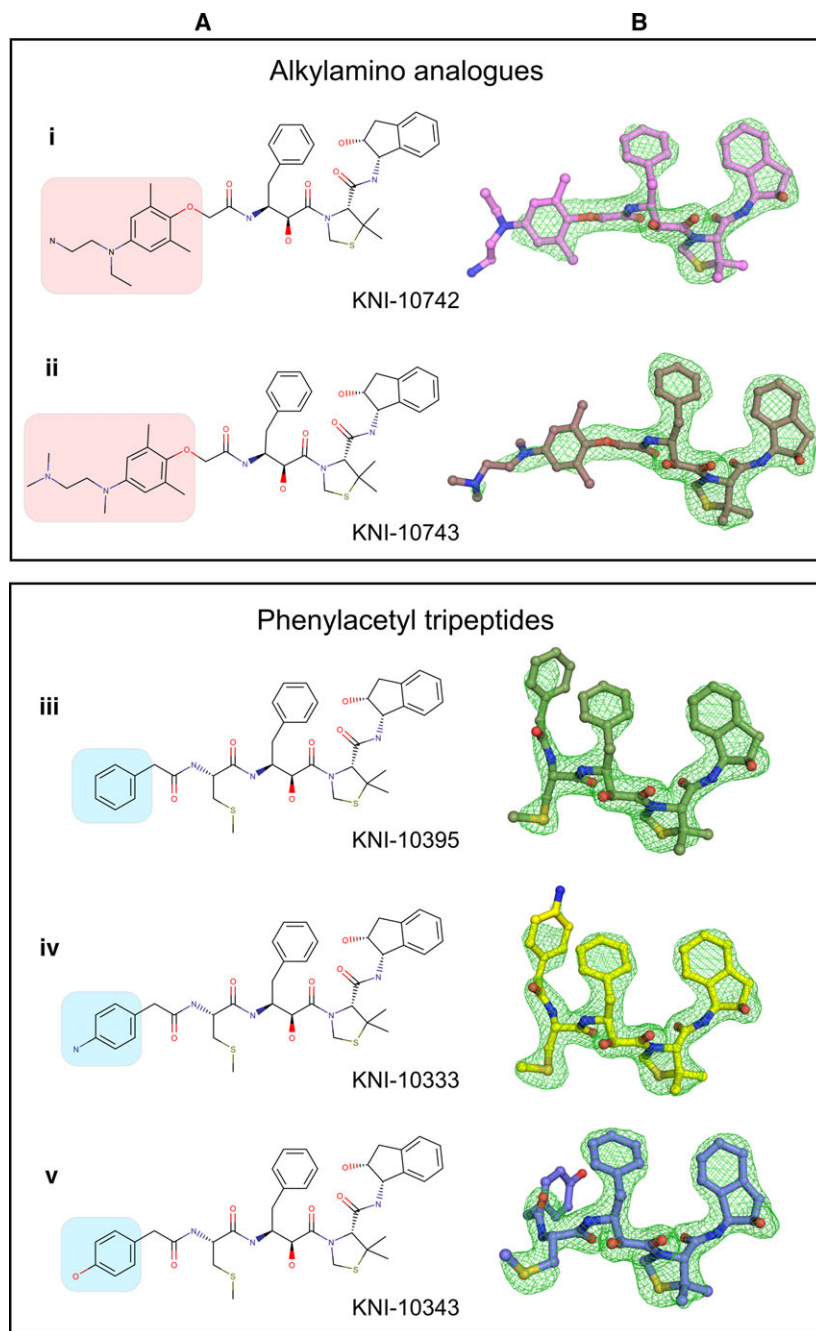


Fig. 3. KNI inhibitors used in this study. (A) Chemical structures of the KNI inhibitors. (B) Omit $F_o - F_c$ map (contoured at 2σ level) of the KNI inhibitors bound in the active site of PMII. Top panel represents the alkylamino analogs with terminal alkylamino chain containing (i) dimethyl group in KNI-10742 and (ii) trimethyl substitutions in KNI-10743. Bottom panel represents the phenylacetyl tripeptides consisting terminal phenylacetyl ring with (iii) no substitution in KNI-10395, (iv) *p*-amino substituent in KNI-10333, and (v) *p*-hydroxyl group in KNI-10343. The terminal groups with the functional variability are shaded in orange in the alkylamino analogs and blue in the phenylacetyl tripeptides.

hydrogen bonds with the main chains of Gly218 and Ser220. The same moiety is also stabilized in the S2 hydrophobic pocket composed of Thr219, Thr223, Ile292, and Ile302. The P1' carbonyl oxygen of the Dmt group is hydrogen bonded to Ser81 in the flap and packed in the S1 hydrophobic pocket with the residues Ile34, Tyr79, Phe113, and Ile125. At the P1 site, the central carbonyl oxygen and the hydroxyl group of the Apns moiety make several hydrogen

bonds with the active site residues Asp36 and Asp216; the former is at the hydrogen bond distance with the main chain carbonyl oxygen of Thr219. Gly38 makes a hydrogen bond with the main chain amide of Apns moiety via water and poly(ethylene glycol) (PEG) molecules in KNI-10742 and KNI-10743, respectively. When present in the active site, the sodium ion forms coordinate bonds with the inhibitor as well as with the active site aspartates. The surrounding hydrophobic

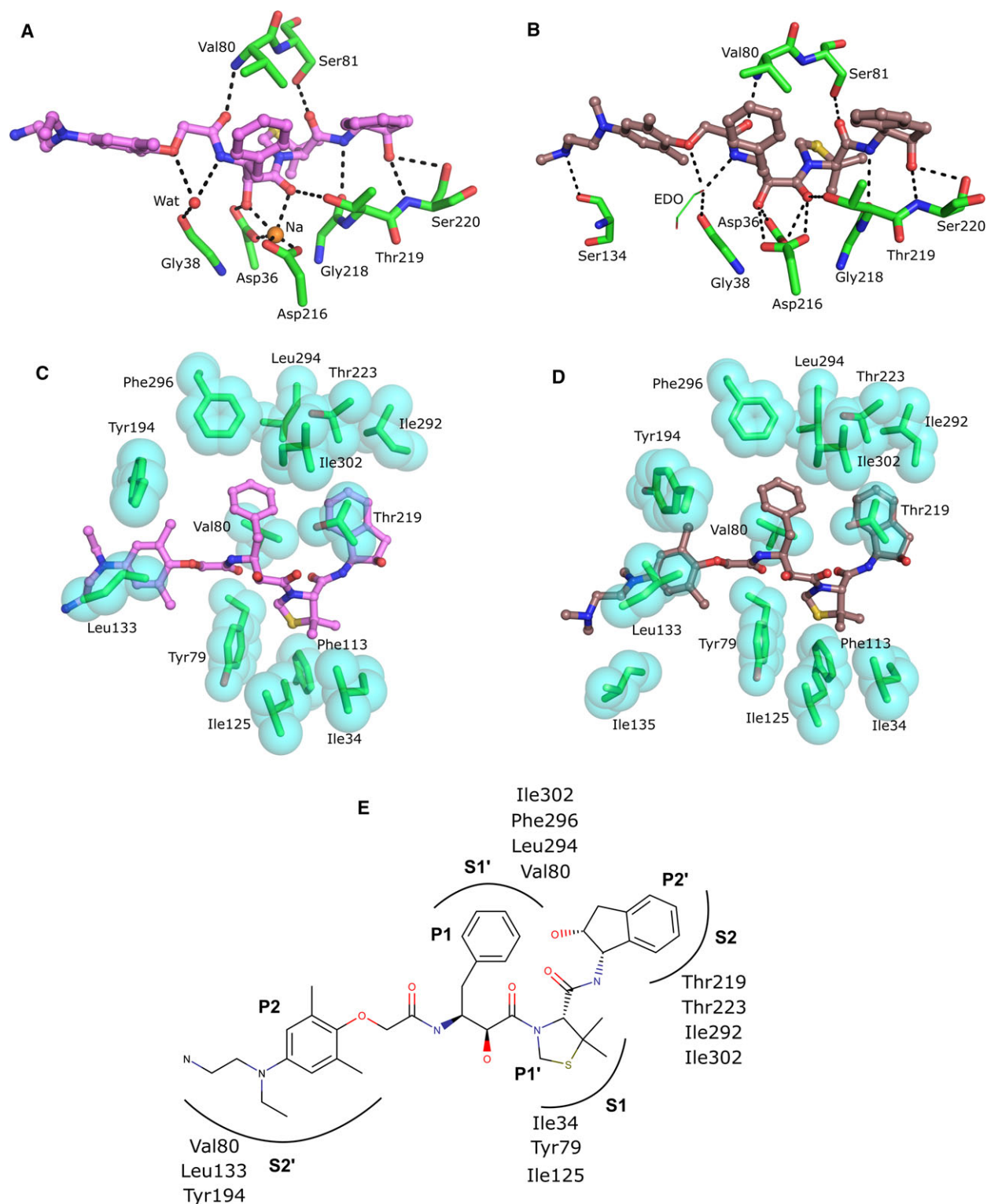


Fig. 4. Interactions present in the active site of complexes of PMII with aminoalkyl analogs. The zoomed-in view of the binding pockets represent the (A, B) hydrogen bonds in black dotted lines and (C, D) hydrophobic interactions as blue spheres in the PMII–KNI-10742 and PMII–KNI-10743 complexes, respectively. The sodium ion is shown as orange sphere in the PMII–KNI-10742 complex. The inhibitors are shown in ball and stick models as magenta carbons in the PMII–KNI-10742 and brown carbons in PMII–KNI-10743 complexes; the residue side chains are shown in sticks. (E) Schematic of the binding mode of KNI-10742 in the active site of PMII.

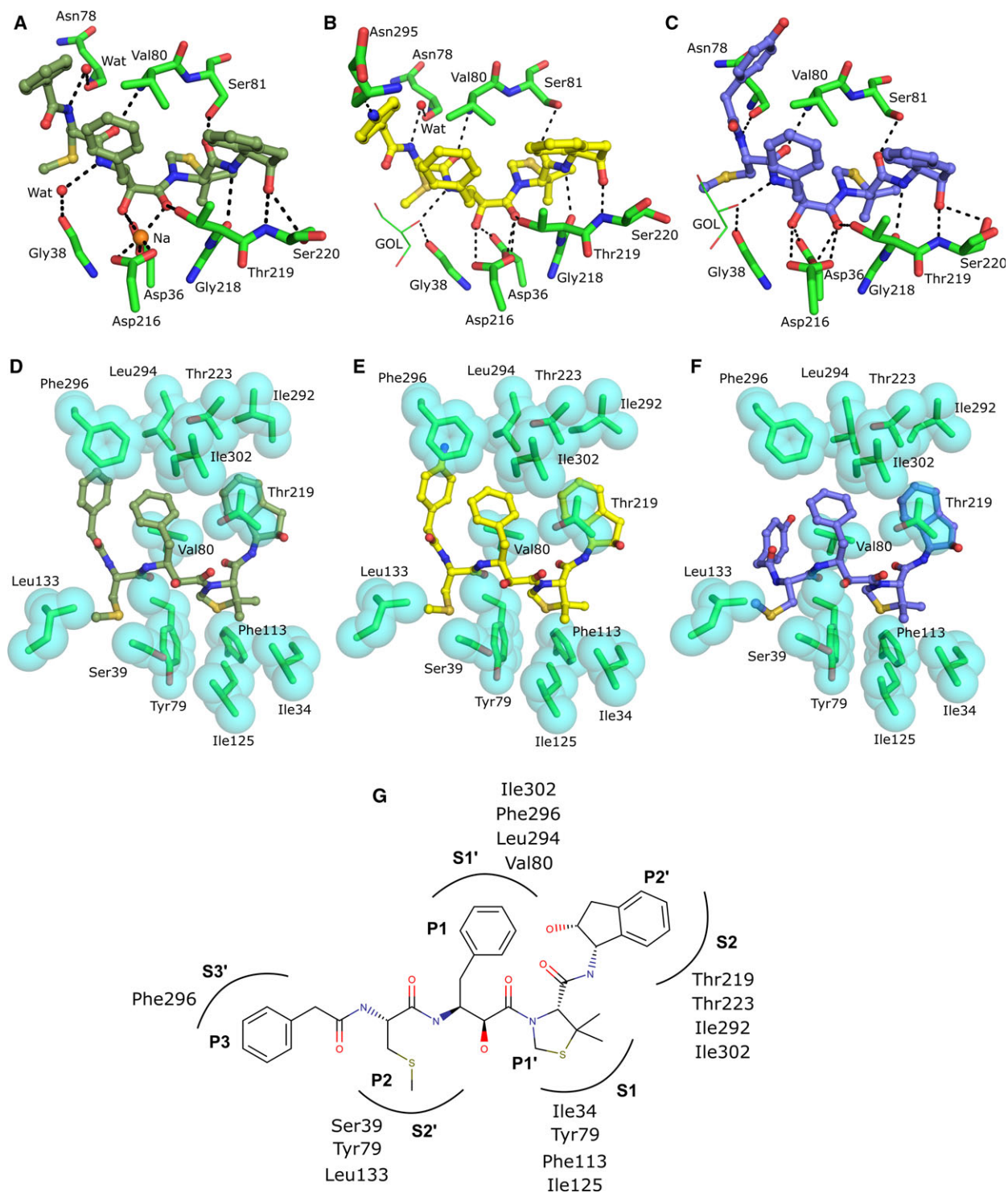


Fig. 5. Active site interactions in complexes of PMII with phenylacetyl derivatives. The zoomed-in view of the binding pockets represent the (A, B, and C) hydrogen bonds in black dotted lines and (D, E, and F) hydrophobic interactions as blue spheres in the PMII–KNI-10395, PMII–KNI-10333, and PMII–KNI-10343 complexes, respectively. The sodium ion is shown as orange sphere in the PMII–KNI-10395 complex. The inhibitors are shown in ball and stick models as dark green, yellow, and blue carbons, in the PMII–KNI-10395, PMII–KNI-10333, and PMII–KNI-10343 complexes, respectively; the residue side chains are shown in sticks. (G) Schematic of the binding mode of KNI-10399 in the active site of PMII.

Table 1. Data collection and refinement statistics of the PMII–KNI inhibitor complex structures.

Data collection ^a	PMII–KNI-10742	PMII–KNI-10743	PMII–KNI-10395	PMII–KNI-10333	PMII–KNI-10343
Space group	<i>I</i> 4	<i>I</i> 4	<i>I</i> 4	<i>I</i> 4	<i>I</i> 4
Unit cell parameters					
<i>a</i> , <i>b</i> , <i>c</i> (Å)	106.6, 106.6, 72.2	106.2, 106.2, 70.8	107.6, 107.6, 72.5	106.5, 106.5, 71.0	106.0, 106.0, 70.8
α , β , γ (°)	90, 90, 90	90, 90, 90	90, 90, 90	90, 90, 90	90, 90, 90
Temperature (K)	100	100	100	100	100
Wavelength (Å)	1.54182	1.54182	0.95372	0.95372	1.54182
Resolution (Å)	40.0–2.1 (2.2–2.1)	40.0–2.15 (2.25–2.15)	40.0–2.1 (2.2–2.1)	40.0–1.9 (2.0–1.9)	40.0–2.0 (2.1–2.0)
R_{merge} (%) ^b	6.5 (125.5)	8.7 (99.9)	6.3 (109.8)	5.6 (123.1)	8.0 (119.6)
Completeness (%)	100 (99.9)	99.9 (99.9)	99.8 (100)	99.7 (99.7)	100 (100)
Mean $I/\sigma(I)$	17.4 (1.8)	16.9 (2.0)	14.4 (1.6)	16.6 (1.5)	16.4 (1.8)
Total reflections	175 209 (22 537)	158 458 (18 793)	120 255 (16 050)	164 828 (23 209)	194 186 (25 702)
Unique reflections	23 705 (3089)	21 566 (2723)	24 239 (3157)	31 284 (4420)	26 651 (3596)
Redundancy	7.4 (7.3)	7.3 (6.9)	5.0 (5.0)	5.3 (5.2)	7.3 (7.2)
Wilson B factor (Å ²)	53.0	47.2	52.0	45.9	44.1
No. of molecules in ASU	1	1	1	1	1
Refinement statistics					
Resolution (Å)	39.0–2.1	39.0–2.15	38.0–2.1	37.0–1.9	37.0–2.0
Working set: no. of reflections	22 516	20 484	23 026	29 717	25 318
R_{factor} (%)	17.3	17.8	18.8	17.8	16.8
Test set: no. of reflections	1185	1078	1212	1565	1333
R_{free} (%)	21.9	19.6	22.5	22.7	20.7
Protein atoms	2623	2623	2643	2630	2623
Water molecule	142	114	113	251	199
CHAPS	2	1	1	1	1
Poly(ethylene glycol)	0	2	0	0	0
Glycerol	0	5	0	4	3
Na ⁺ ion	1	0	1	0	0
Geometry statistics					
r.m.s.d. bond distance (Å)	0.012	0.010	0.010	0.010	0.010
r.m.s.d. bond angle (°)	1.75	1.53	1.60	1.66	1.64
Isotropic average B-factor (Å ²)					
Protein	34.7	30.2	30.5	30.8	29.5
Solvent	53.9	49.8	59.8	56.0	51.7
Ligand	50.9	48.7	47.4	38.3	38.6
Ramachandran plot (%)					
Most favored region	96.4	97.3	96.1	97.3	96.1
Allowed regions	3.6	2.7	3.9	2.7	3.6
Outlier	0	0	0	0	0.3
PDB code	5YIE	5YIB	5YID	5YIC	5YIA

^aValues in parentheses correspond the highest resolution shell

^b $R_{\text{merge}} = \sum |I - \langle I \rangle| / \sum I$ where I is the observed integrated intensity, $\langle I \rangle$ is the average integrated intensity obtained from multiple measurements, and the summation is over all observed reflections.

residues Val80, Leu294, Phe296, and Ile302 tightly hold the phenyl group of the Apns moiety in the S1' hydrophobic pocket. The 2,6-dimethylphenoxyacetyl moiety present at the P2 position engages in a hydrogen bond with Val80 in the flap region as well as is stabilized by Leu133 and Tyr194 in the S2' pocket. Due to variations at the P2 positions, KNI-10743 makes an additional hydrogen bond and a hydrophobic interaction with Ser134 and Ile135, respectively, compared to KNI-10742 (Fig. 4A–D).

Crystal structures of PMII complexed with KNI inhibitors containing phenylacetyl derivatives (KNI-10395, KNI-10333, and KNI-10343)

KNI-10395, KNI-10333, and KNI-10343 have 2-methylsulfanyl moiety with methylthioalanine group (Mta) at the P2 position next to the P1 site, similar to KNI inhibitors developed against HIV proteases [40]. At the P3 position, the phenylacetyl ring has no substitution in KNI-10395, a ρ -amino substituent in

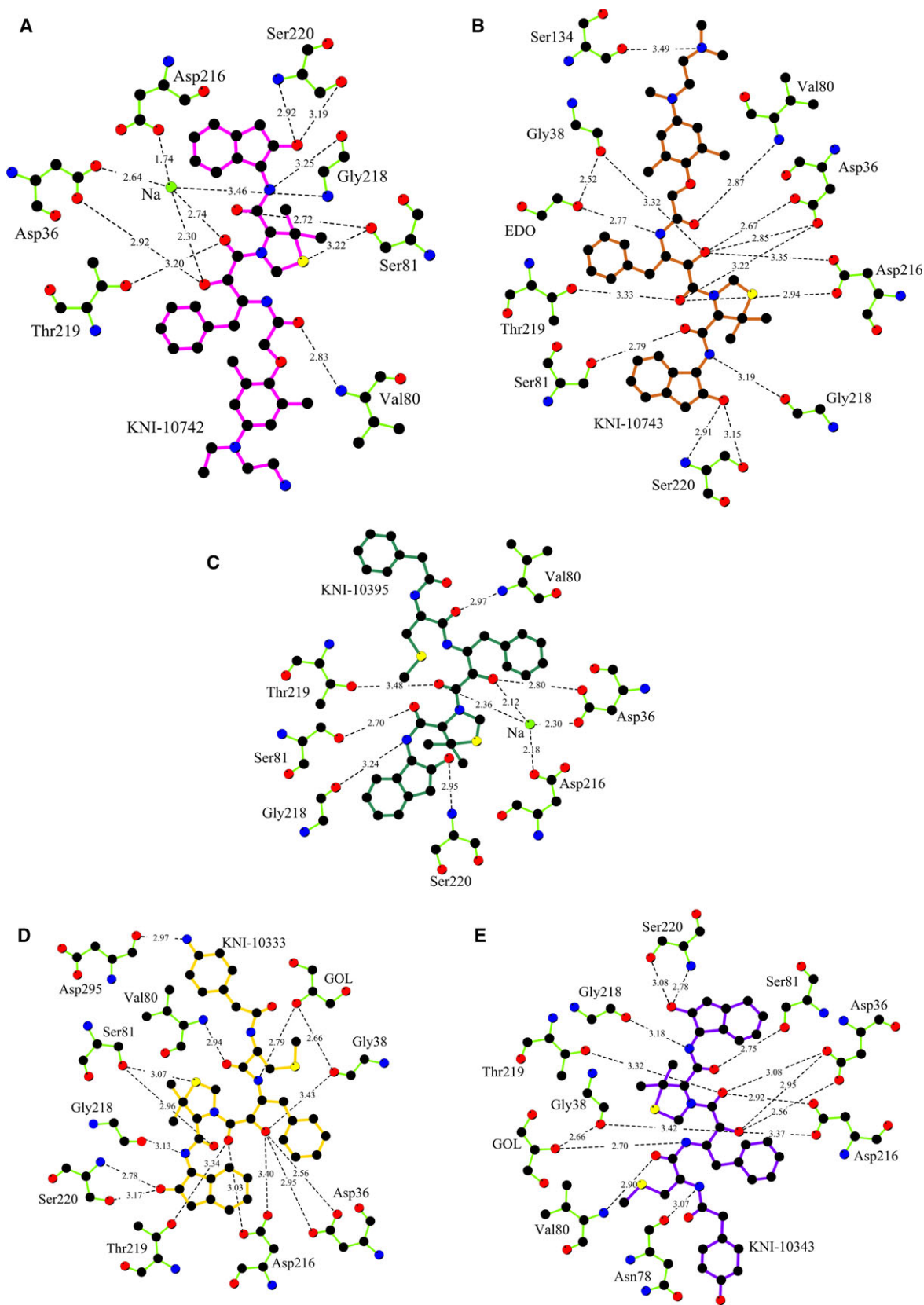


Fig. 6. The schematic representation of the hydrogen bond distances in PMII–KNI inhibitor complexes analyzed by LIGPLOT. The hydrogen bond distances are shown as black dotted lines (Å) in the active sites of PMII in complexes with (A) KNI-10742 (magenta bonds), (B) KNI-10743 (brown bonds), (C) KNI-10395 (dark green bonds), (D) KNI-10333 (yellow bonds), and (E) KNI-10343 (purple bonds). The amino acid residues are shown with light green bonds. The carbon, nitrogen, oxygen, and sulfur atoms in the inhibitors and residues are shown as black, blue, red, and yellow spheres, respectively. The sodium ion is shown as green sphere in PMII–KNI-10742 and PMII–KNI-10395 complexes.

KNI-10333, and a *p*-hydroxyl group in KNI-10343 [Fig. 3A (iii–v)]. The structures of the complexes of PMII with KNI-10395, KNI-10333, and KNI-10343 have been solved with data extending to 2.1, 1.9, and 2.0 Å resolution, respectively. The data collection and refinement statistics for these structures are presented in Table 1. The omit $F_o - F_c$ maps show the presence of bound inhibitors in the active site of PMII [Fig. 3B (iii–v)]. No evidence of a sodium ion is found in the complexes of PMII with KNI-10333 and KNI-10343, which were crystallized in conditions without sodium. Superposition of 327 $C\alpha$ atoms of the PMII–KNI-10395 structure with the PMII–KNI-10333 and PMII–KNI-10343 complexes yielded r.m.s.d. values of 0.25 and 0.30 Å, respectively, indicating slight changes in the geometry of the aspartates and the central hydroxyl group of the inhibitor in the presence or absence of sodium. Several hydrogen bonds and hydrophobic interactions responsible for stabilizing the inhibitors in the active site (Fig. 5A–G) were further analyzed by LIGPLOT v.1.4.5 (Fig. 6C–E). In the PMII–KNI-10395 complex, the sodium ion makes close contacts with the inhibitor as well as with the catalytic aspartates. Most of the interactions are conserved at the P1' and P2' sites, with maximum variability seen at the P2 and P3 positions in these PMII–KNI inhibitor complexes.

In the PMII–KNI-10395 and PMII–KNI-10333 complexes, the main chain amide and carbonyl groups of Mta moiety form hydrogen bonds with the main chain carbonyl of Asn78 through a water molecule and the flap residue Val80, respectively (Fig. 5A,B). However, Asn78 forms a direct hydrogen bond with Mta moiety in PMII–KNI-10343 complex due to the movement of the phenylacetyl ring toward the flap region comprising Asn78, Tyr79, and Val80 (Fig. 5C, F). The amino substituent of the phenylacetyl moiety in KNI-10333 creates an additional hydrogen bond with Asp295 (Fig. 5B), which is not seen in KNI-10343 bound PMII structure (Fig. 5C). Interestingly, multiple conformations of Tyr194 in various PMs-inhibitors complexes [29,41] suggest that the flexible nature of this residue is important for its interaction with different P2–P3 groups, which might have implications for antimalarial drug design.

Structural basis of the higher inhibition potency of KNI-10743 and KNI-10333

A comparison of the crystal structures of PMII–KNI inhibitor complexes provides molecular insights explaining the higher potency of some of these inhibitors. KNI-10743 has a more extended alkyl chain compared to KNI-10742, with an amino substituent at the P2 position that makes an additional hydrogen bond (3.4 Å) with the carbonyl oxygen of Ser134 in PMII and which is stabilized by the side chain of Ile135. The electron density of the alkylamino chain was comparatively weak, indicating its intrinsic flexibility that could result in strong polar interactions with the main chains of Asp132 and Ser134 along with the hydrophobic interaction with the side chain of Leu133 (Fig. 7A). The electrostatic potential surface of PMII–KNI-10743 complex shows that the alkylamino chain of KNI-10743 is stabilized in the negatively charged pocket (Fig. 7C).

The crystal structure complexes of PMII with phenylacetyl tripeptides, KNI-10395, KNI-10333, and KNI-10343 clearly indicate that the ring substituents of the inhibitors govern the orientation of the phenylacetyl group, thus resulting in the novel interactions at the P3 position. In the PMII–KNI-10333 complex, there is an additional hydrogen bond formed between the *p*-amino group of the phenylacetyl ring and the main chain of Asp295 in the S3' pocket, which might be the primary determinant for the higher inhibitory activity of KNI-10333 (Fig. 7B). The structure of PMII–KNI-10333 complex demonstrates that the *p*-amino group of the phenylacetyl ring is stabilized in the negative pocket, whereas stabilization of the negatively charged oxygen at the phenyl ring in the PMII–KNI-10343 complex is not possible in this pocket (Fig. 7D).

Inhibition of PMI and PMIV by KNI-10743 and KNI-10333

As inhibitory activities of KNI-10743 and KNI-10333 against PMII were highly encouraging, we measured their inhibition potency for mature PMI, HAP, and PMIV proteins. KNI-10743 and KNI-10333 strongly inhibit PMI with the nanomolar inhibition constants of 12.6 and 0.47 nM, respectively (Fig. 8A,C).

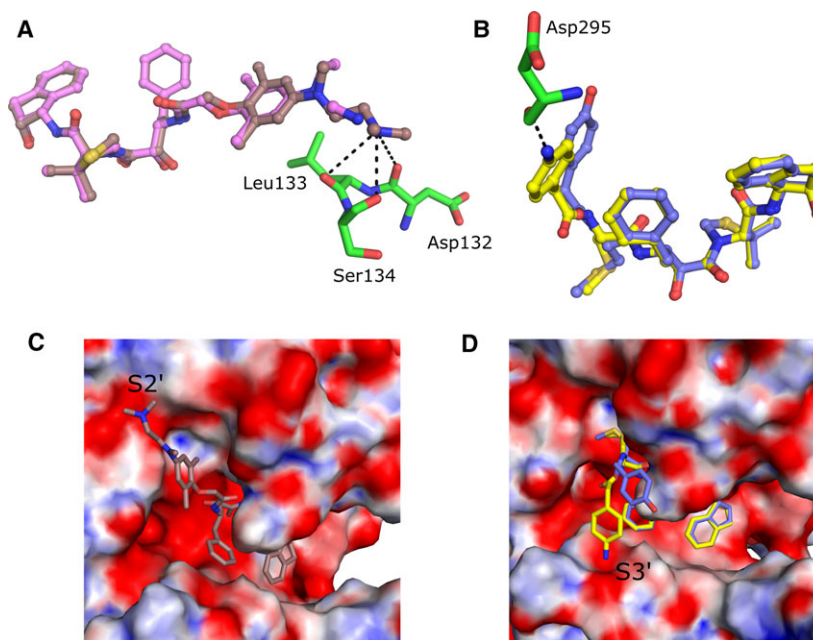


Fig. 7. Structural basis of the inhibitory potency of the KNI-10743 and KNI-10333. (A) Superposition of KNI-10742 (magenta carbon) and KNI-10743 (brown carbon) in the active site of PMII. KNI-10743 has an additional weak hydrogen bond with Ser134 and the flexibility of alkylamino chain creates the propensity to interact strongly with other surrounding residues, Asp132 and Leu133 represented by the black dotted lines. (B) Superposition of KNI-10333 (yellow carbon) and KNI-10343 (blue carbon) in the active site of PMII. KNI-10333 makes an additional polar interaction with Asp295 as represented by the black dotted line. The inhibitors are shown in ball and stick models; the residue side chains are shown in sticks. (C) The zoomed-in view of the electrostatic surface diagram of PMII in complex with KNI-10743 (shown as stick) shows the stabilization of aminoalkyl chain in the negatively charged pocket. (D) The zoomed-in view of the electrostatic surface diagram of superposed complexed structures of PMII–KNI-10333 and PMII–KNI-10343 showing the stabilization of phenylacetyl ring in KNI-10333 (yellow carbon) in the negatively charged binding pocket while the same ring is moved away in KNI-10343 (blue carbon) and is not stabilized in this binding pocket. The red, blue, and white colors on the surface representation indicate the negatively, positively, and neutral charged regions on PMII, respectively.

KNI-10743 and KNI-10333 block the activity of PMIV with the K_i values of 26 and 6 nM, respectively (Fig. 8B, C). Inhibition studies on mature HAP were also performed; however, limited data were obtained due to very low amount of the active protein. Nonetheless, the nanomolar inhibitory activities of KNI-10743 and KNI-10333 against PMI, PMII, and PMIV (Fig. 8C) signify the ability of these compounds to effectively impede the actions of multiple vacuolar PMs.

Antiparasitic and cytotoxicity assays of KNI-10743 and KNI-10333

Besides an *in vitro* inhibition assay of KNI-10743 and KNI-10333 against three vacuolar PMs (PMI, PMII, and PMIV), the efficacy of these inhibitors in killing malaria parasites was also investigated. The cultures of *P. falciparum* were treated with different concentrations of these compounds ranging from 0.01 to 5.0 μ M. Treatment with either compound shows that the parasites progress through the asexual cycle; however, the

rings at 48–96 h look unhealthy and pyknotic, with low IC_{50} values of 0.43 and 0.93 μ M for KNI-10743 and KNI-10333, respectively [Fig. 9A (ii and iii), B]. The solvent control (0.2% v/v DMSO) has no visible adverse effect on the cultures [Fig. 9A (i)].

Furthermore, the inhibitory effect of KNI compounds on the process of Hb degradation mediated by PMs was studied inside the parasite. The SDS/PAGE clearly shows a significant accumulation of undigested Hb in the parasites treated with KNI inhibitors, but degraded Hb (smeared band at \sim 14 kDa) in the untreated parasites (Fig. 9C). This result proves that KNI compounds gain entry into the food vacuole of the parasite, thus are able to inhibit PMs and suppress the Hb degradation pathway.

The cytotoxicity of KNI inhibitors was also evaluated by the cell viability 3-(4,5-dimethylthiazol-2-yl)-2,5-diphenyltetrazolium bromide (MTT) assay. The morphology of cells in the presence of KNI-10743 and KNI-10333 remains intact when compared to cisplatin-treated cells (Fig. 9D). Both inhibitors show no

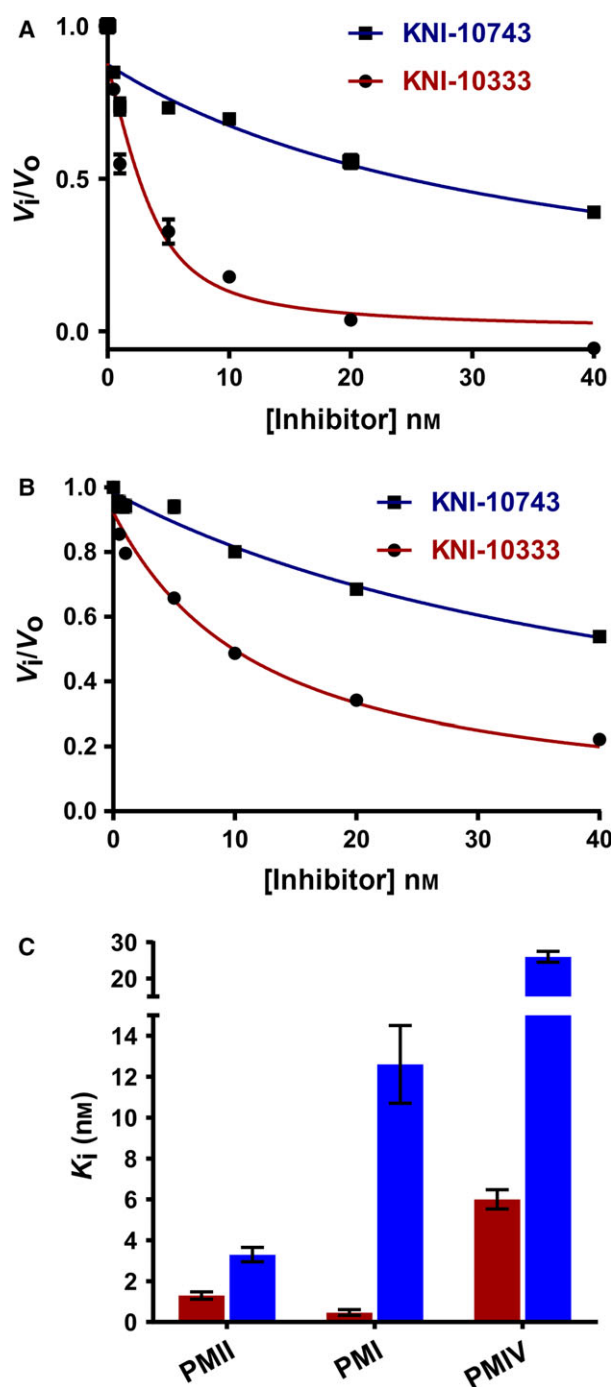


Fig. 8. Inhibition of the vacuolar PMs by KNI inhibitors. (A) Plot showing the inhibition of PMI by KNI-10743 and KNI-10333. (B) Plot showing the inhibition of PMIV by KNI-10743 and KNI-10333. (C) The bar graphs comparing the K_i values of KNI-10743 (blue bar) and KNI-10333 (brown bar) against PMII, PMI, and PMIV. The experiments are performed in triplicate ($n = 3$) and the error bars represent \pm SEM.

significant cytotoxicity at the highest concentration tested (25 μ M, continuous exposure for two consecutive days) on human foreskin fibroblasts (HFF; Fig. 9E).

Discussion

The vacuolar PMs are essential enzymes for the survival of malarial parasite and hence are considered as important antimalarial drug targets. Nevertheless, the use of these enzymes for structure-based antimalarial drug development has been hindered, primarily due to the difficulty in their soluble expression. Here, the successful preparation of soluble forms of the four vacuolar PMs is achieved. We have performed structural studies on PMII in which we used, for the first time, the protein which was expressed in a soluble form. In addition, our study reports multiple PMII structures in complexes with a number of potent KNI compounds, to identify the lead inhibitors for further modifications.

The soluble mature forms of PMI, PMII, and PMIV were used to evaluate the inhibition kinetics of the KNI compounds. KNI-10743 and KNI-10333 have inhibitory activities in the low nanomolar range against multiple vacuolar PMs, which is very promising since PMI and PMII are primarily responsible for the initial cleavage of Hb [8]. Furthermore, PMIV is conserved across various *Plasmodium* species; therefore, strong inhibition of PMIV provides an opportunity to combat other infectious *Plasmodium* species as well. We have reported five cocrystal structures of KNI inhibitors bound to PMs that provide an effective starting point for future antimalarial drug development. KNI-10743 and KNI-10333 exhibit significantly low IC_{50} values. In addition, it was demonstrated that these inhibitors reach the food vacuole by crossing multiple membranes and halt Hb degradation by inhibiting the activity of PMs, resulting in killing of the parasite. Such direct evidence emphasizes the drug-like properties of these compounds. Furthermore, our results show that these KNI inhibitors do not elicit cytotoxic effects in human cells.

The extensive structural analysis of the PMII–KNI inhibitor complexes has been performed in order to better understand the basis of their differential potency. KNI-10743 has the flexible aminoalkyl chain at its P2 position that interacts with the main chain of Ser134 when compared to KNI-10742. The phenylacetyl ring at the P3 position in KNI-10333 and KNI-10343 modulates the orientation of the ring to create

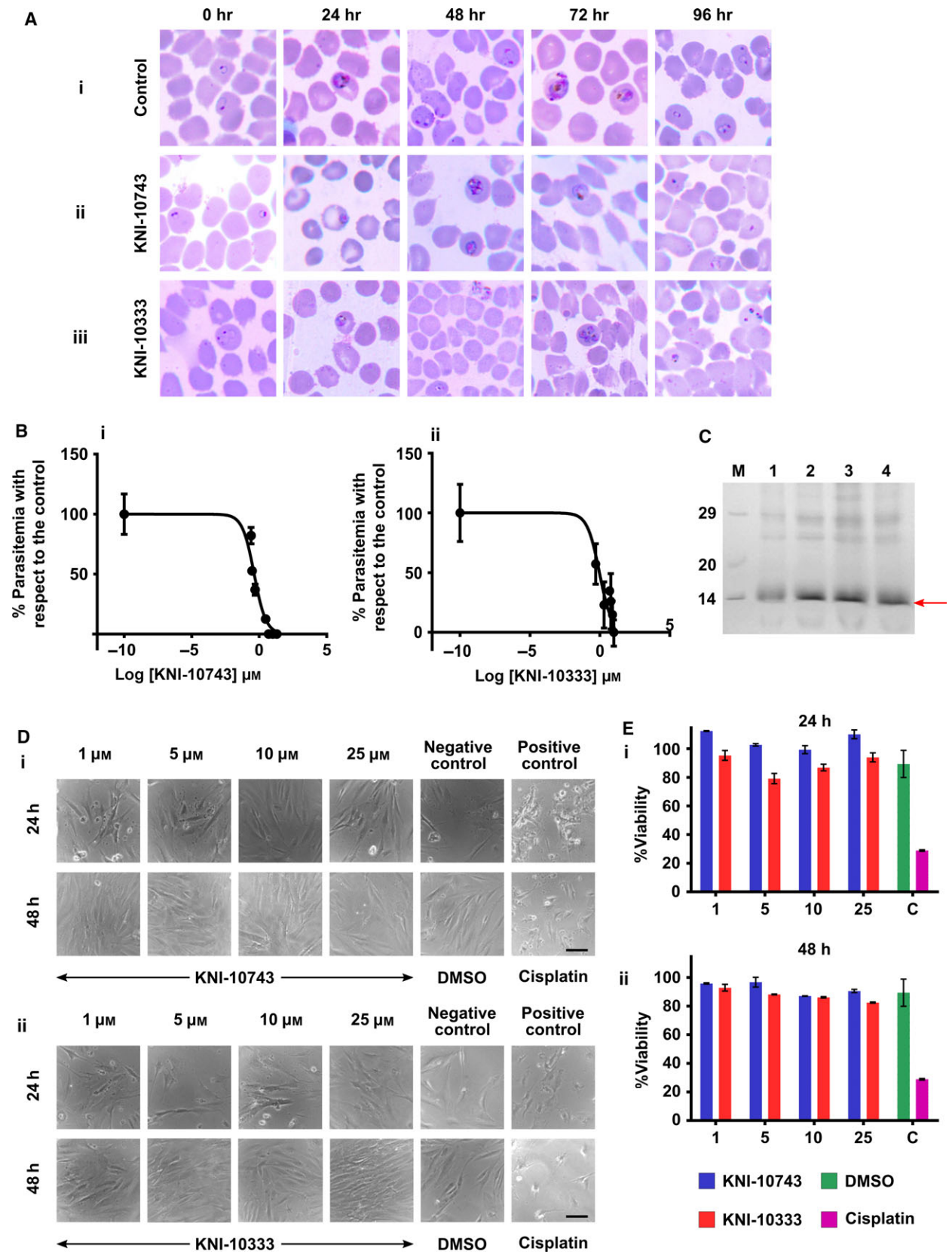


Fig. 9. Antiparasitic activity and cytotoxicity of KNI-10743 and KNI-10333 inhibitors. (A) Morphological changes in *Plasmodium falciparum* 3D7 treated with the KNI inhibitors monitored by Giemsa-stained blood smears at five different time points (0–96 h) after drug administration. (B) Log concentration of (i) KNI-10743 and (ii) KNI-10333 versus percentage parasitemia with respect to control. The experiments are performed in triplicate ($n = 3$) and the error bars represent \pm SEM. (C) SDS/PAGE showing significantly higher amount of the undigested Hb (marked with arrow at ~ 14 kDa) in *P. falciparum* treated with the KNI inhibitors suggesting that the administration of drugs directly prevent the Hb degradation by the parasites. Hb degradation in the lanes depicts parasites treated with Lane 1: DMSO (negative control), Lane 2: chloroquine (positive control), Lane 3: KNI-10743, Lane 4: KNI-10333. Lane M represents the protein molecular weight (kDa) marker. (D) Microscopic images showing the morphological changes in the HFF upon treatment with (i) KNI-10743 and (ii) KNI-10333. Scale bar, 50 μm . (E) Percentage viability of the HFF exposed to KNI-10743 (blue), KNI-10333 (red), negative control DMSO (green), and positive control cisplatin (magenta) after (i) 24 h and (ii) 48 h. The experiments are performed in triplicate ($n = 3$) and the error bars represent \pm SEM.

novel hydrogen-bonding contacts. The hydrogen bond between the amino group of phenylacetyl moiety of KNI-10333 and main chain Asp295 of PMII may be responsible for its higher inhibitory activity compared to the other inhibitors.

Due to the lack of proper structural data, most of the previous modifications in the KNI inhibitors examined the P2 and P3 sites, based on analysis of the binding mode of similar peptidomimetic compounds to other pepsin-like aspartic proteases [24,25]. For these reasons, the resulting compounds were not very well stabilized in their respective binding pockets. Analysis of the crystal structures of the complexes presented herein suggests that extension of the KNI inhibitors toward the P2' site could provide one of the expedient routes to discover unexplored binding pockets of vacuolar PMs.

Taken together, our detailed biochemical and structural data provide a new and progressive way to create potent derivatives of KNI-10743 and KNI-10333 targeting multiple vacuolar PMs, and possibly nonvacuolar PMs as well, thus making them promising candidates for future clinical trials.

Materials and methods

Expression of the vacuolar PMs

The truncated PMII (Lys77P-Leu329) was cloned between NcoI and XhoI sites in the pET32b vector with a Trx tag at the N terminus (Trx-tPMII; Fig. 1A) [42] to improve the solubility of the protein. The *E. coli* Rosetta-gami B (DE3) pLysS competent cells were transformed with the expression construct containing Trx-tPMII fusion gene and grown overnight at 37 °C in 50 mL LB with 50 $\mu\text{g}\cdot\text{mL}^{-1}$ ampicillin, 34.1 $\mu\text{g}\cdot\text{mL}^{-1}$ chloramphenicol, 12.5 $\mu\text{g}\cdot\text{mL}^{-1}$ kanamycin, and 12.5 $\mu\text{g}\cdot\text{mL}^{-1}$ tetracycline. The overnight grown culture was used to inoculate fresh LB supplemented with the antibiotics as above and cells were grown at 37 °C in a shaker until the OD₆₀₀ reached 1.0. The protein was overexpressed by inducing the culture with 1 mM IPTG and the cells were further grown at 30 °C for 5–6 h. The cells were

collected by centrifugation at 6000 *g* at 4 °C for 10 min and the pellet was used for protein purification. Cloning of the Trx-tPMIV fusion gene along with the expression of the recombinant Trx-tPMI, Trx-tHAP, and Trx-tPMIV fusion proteins were performed as described for PMII.

Purification and activation of the vacuolar PMs

The purification of PMII was performed as described previously [43], with some modifications to the protocol. The cells were suspended in a lysis solution containing 50 mM sodium phosphate buffer, 0.3 M NaCl, 1.0 $\text{mg}\cdot\text{mL}^{-1}$ lysozyme, 10 $\mu\text{g}\cdot\text{mL}^{-1}$ DNase, 10 mM MgCl₂, and 0.2% CHAPS detergent [Sisco Research Laboratories Pvt. Ltd. (SRL), Mumbai, India], pH 7.4. The cell suspension was kept at room temperature for 4 h with gentle shaking. The supernatant was separated by centrifugation at 16 000 *g* and filtered through a 0.45 μm poly(vinylidene difluoride) membrane. The soluble fraction was loaded on to the Ni-NTA affinity column (GE Healthcare, Chicago, IL, USA) pre-equilibrated with 50 mM sodium phosphate buffer, 0.3 M NaCl, and 10 mM imidazole, pH 7.4. The column was thoroughly washed with a buffer containing 50 mM sodium phosphate, 0.3 M NaCl, 25 mM imidazole, pH 7.4 to remove the nonspecific impurities from the column. The bound proteins were eluted using increasing imidazole concentrations (75, 125, and 250 mM). The Trx-tPMII containing fractions were pooled and concentrated using 10 kDa centrifugal cut-off device as well as purified by the Superdex 75 16/600 gel-filtration (GE Healthcare) column equilibrated in 50 mM sodium phosphate buffer and 0.15 M NaCl along with 0.2% CHAPS, pH 7.4. The purity level of the eluted fractions at each stage of purification was examined by SDS/PAGE. Protein estimation was done using the Bradford method [44].

During the purification and concentration of fusion protein in 50 mM phosphate buffer, 0.15 M NaCl, and 0.2% CHAPS, pH 7.4, the Trx tag got removed from the N terminus of the protein, resulting in the tPMII zymogen. The tPMII protein was autoactivated when mixed with a four-fold volume of 0.1 M sodium acetate pH 4.5, followed by an incubation at 37 °C for 4 h. The complete activation of tPMII was monitored on SDS/PAGE. The purification and

activation of PMI, HAP, and PMIV were carried out similarly as done for PMII.

Synthesis of the KNI inhibitors

The inhibitors used in this study were synthesized from an Apns-containing intermediate as previously reported [24,25]. Briefly, the alkylamino analogs, KNI-10742 and KNI-10743, were prepared from the Apns-containing intermediate by coupling with 2,6-dimethylphenoxyacetic acid which has the corresponding substituted 2-aminoethylamino group, following deprotection of the Boc group, additionally methylating for KNI-10743. For phenylacetyl tripeptides, the intermediate was coupled with Boc-Mta-OH using *N*-ethyl-*N*α-[3-(dimethylamino)propyl]carbodiimide hydrochloride (EDC-HCl) plus 1-hydroxybenzotriazole. After removal of the Boc group using HCl-dioxane, the corresponding phenylacetic acids were combined with benzotriazol-1-yloxy-tris(dimethylamino)phosphonium hexafluorophosphate to give the tripeptidic KNI-10343 and KNI-10395. Further deprotection of the Boc-protected phenylacetyl group was performed to obtain KNI-10333. All the crude products were purified and analyzed by HPLC with > 95% purity and identified by MALDI-TOF MS.

Enzyme activity and inhibition studies

For Hb degradation assay, the preactivated PMII was mixed with Hb and sodium acetate (0.1 M, pH 4.5) and incubated at 37 °C for 4 h. Degradation of Hb was assessed by 15% SDS/PAGE.

Quantitative estimation of the proteolytic activity of mature PMII utilized the internally quenched fluorescent synthetic peptide substrate EDANS-CO-CH₂-CH₂-CO-Ala-Leu-Glu-Arg-Met-Phe-Leu-Ser-Phe-Pro-Dap-(DABCYL)-OH, with a cleavage site between Phe-Leu (AnaSpec Inc., Fremont, CA, USA) [45]. Stock solutions of the internally quenched substrates were prepared in 100% DMSO. The increase in fluorescence during substrate cleavage was monitored using a Jasco 8500 fluorimeter. The mature PMII was mixed with the 0.1 M sodium acetate buffer pH 5.0 and the reaction was initiated by the addition of the substrate in the reaction mix. The final substrate concentration ranged from 0.1 to 5.0 μM. Each experiment was performed in triplicate. An increase in fluorescence intensity was measured as a function of time at an excitation maximum of 335 nm and emission was recorded at a maximum of 500 nm with the 5 nm slit widths at 25 °C. The initial velocity, measured as fluorescence intensity per unit time (I_t), was calculated from the slope during the linear phase of cleavage till 60 s by a linear regression fit in GRAPHPAD PRISM software (Version 6.01; GraphPad Software, La Jolla, CA, USA). Initial velocities were converted from the units of fluorescence (I_t) to the concentration per unit time (V_o in μmol·min⁻¹) using the equation derived from the

fluorescence intensity obtained for various known EDANS concentrations. The K_m value was derived from the nonlinear regression by fitting the initial velocity to a Michaelis-Menten model using GRAPHPAD PRISM software.

Inhibition assays were performed in triplicate as previously described [46] with various KNI compounds (KNI-10742, KNI-10743, KNI-10395, KNI-10333, and KNI-10343), as well as with pepstatin A, with a few modifications to the protocol. The enzyme was pretreated with the compounds at various concentrations (0.5–40 nM) at 25 °C for 5 min in the assay buffer containing 0.1 M sodium acetate pH 5.0, followed by the addition of subsaturating concentration of a substrate. The activity of the enzyme without the inhibitor was considered as 100% and referred to as V_o . Hydrolysis of the substrate was monitored at each inhibitor concentration to obtain V_i values. The V_i/V_o values were fitted to the Morrison equation [47] in GRAPHPAD PRISM to determine the K_i values. The inhibitory activities of KNI-10743 and KNI-10333 were estimated for both PMI and PMIV. The concentration of PMI and PMIV used were 2 nM. The assays and the calculations for PMI and PMIV were performed similarly as described for PMII.

Crystallization and data collection

The pure mature PMII was mixed with a threefold molar excess of inhibitor and the mixture was incubated at 4 °C overnight. For crystallization experiments, the protein-ligand complex was buffer exchanged in a fivefold volume of 50 mM phosphate buffer containing 0.15 M NaCl, 0.2% CHAPS, pH 7.4, and concentrated to 7–10 mg·mL⁻¹ using 10 kDa cut-off centrifugal device.

Crystallization screens of the PMII-KNI inhibitor complexes were set up using the sitting-drop vapor diffusion method at 293 K with a Phoenix crystallization robot. Initially, crystals of PMII complexed with KNI-10742 and KNI-10395 were obtained within a week in 0.1 M HEPES pH 7.5 and 1.4 M sodium citrate tribasic dihydrate. Crystals of the PMII-KNI-10743, PMII-KNI-10333, and PMII-KNI-10343 complexes were grown in 0.2 M lithium sulfate, 1.26 M ammonium sulfate, 0.1 M Tris pH 8.5. On optimization of the crystallization set up using the hanging drop vapor diffusion method, high quality crystals were grown within 2 days. For data collection, the crystals were briefly transferred to the cryoprotectant solution and then to the liquid nitrogen stream at 100 K. The cryoprotectant used to freeze all the crystals of PMII-KNI inhibitor complexes was the mother liquor containing 30% glycerol, except for the PMII-KNI-10743 complex, in which case both glycerol and poly(ethylene glycol) were used. The data sets for three of the inhibitor bound PMII complexes (KNI-10742, KNI-10743, and KNI-10343) were collected by the rotation method using a home X-ray radiation source consisting of a Rigaku Micromax 007HF generator equipped with *R*-Axis IV++ detector at the Protein Crystallography Facility,

IIT Bombay. The data sets for the other two PMII-inhibitor complexes (PMII-KNI-10395 and PMII-KNI-10333) were collected at beamline BM14 of the European Synchrotron Radiation Facility (ESRF, Grenoble, France) using a MarCCD detector. The data sets were indexed and integrated using the program *xds* [48]. Integrated intensities were converted to structure factors with the modules *F2MTZ* and *CAD* of *CCP4* [49]. The data collection statistics are presented in Table 1.

Structure solution and refinement

The Matthews' coefficient [50] for all crystals indicated the presence of one molecule in the asymmetric unit. The coordinates of the protein part of the PMII-pepstatin A complex structure (PDB ID: 1XDH) were initially used as the search model to solve the PMII-KNI-10395 structure. Subsequently, PMII-KNI-10395 structure was used to solve the other complexed structures by molecular replacement with the program *PHASER* [51]. After the first cycle of refinement of the model in *REFMAC5* [52], the sigma-A weighted $F_o - F_c$ electron density maps indicated the presence of an inhibitor in the active site pocket of PMII. The *ELBOW* program module [53] of *PHENIX* [54] was used to generate the geometry restraints for all inhibitors. After placing the inhibitor in the active site of PMII, iterative cycles of refinements with *REFMAC5* and manual model building in the electron density map using *COOR* [55] were carried out. Water and other solvent molecules were progressively added at the peaks of electron density higher than 3σ in sigma-A weighted $F_o - F_c$ maps while monitoring the decrease of R_{free} and improvement of the overall stereochemistry of the model. The analysis made by *CheckMyMetal* server (https://cs.gid.org/metal_sites) was used to confirm the presence of sodium ions in PMII complexed with KNI-10742 and KNI-10395 crystallized in mother liquor containing high concentration of sodium salt. Local anisotropy was modeled with translation-libration-screw (TLS) parameters by dividing the protein molecule into distinct TLS groups [56]. The first few N-terminal residues in an asymmetric unit could not be modeled due to the lack of proper electron density. The final refinement statistics and validation parameters of the determined structures were obtained with *MolProbity* [57] and are summarized in Table 1. All structure-related figures were generated with *PYMOLE* (<https://www.pymol.org/>).

Antiparasitic assay

The laboratory-adapted *P. falciparum* 3D7 strain was grown with human O^+ erythrocytes in RPMI-1640 (Gibco, Dublin, Ireland) supplemented with 25 mM HEPES pH 7.5, 25 mM sodium bicarbonate, 50 mg·L⁻¹ hypoxanthine, 0.2% D-glucose, 5% albumax II, and 40 µg·mL⁻¹

gentamicin [58,59]. The cultures were incubated at 37 °C in a gas chamber of 5% CO₂, 1% O₂, and 94% N₂. Cultures were maintained by changing the medium every 24 h. Synchronization was achieved by 5% D-sorbitol [60]. The inhibitors, KNI-10743 and KNI-10333, were diluted in a concentration range of 0.01–10 µM in 2 mL culture volume. The parasite culture with 0.2–0.5% synchronized rings (3% hematocrit) was seeded in the 24-well tissue culture plate and incubated up to 96 h. The percentage parasitemia was determined microscopically after Giemsa staining by counting the parasites per 500 erythrocytes in the blood smears. The concentration of inhibitors that inhibit 50% of parasite growth was calculated by linear interpolation using the *GRAPHPAD PRISM* software by plotting the Log of the concentration of the inhibitor versus percentage response.

Monitoring the effect of KNI inhibitors on hemoglobin degradation inside *P. falciparum*

The Hb degradation inside *P. falciparum* was monitored as previously described with a few modifications to the protocol [61,62]. For this, the parasite culture in the late ring stage (at 10% parasitemia) was incubated with 2.7 µM KNI-10743 and 1.2 µM KNI-10333 for 10–12 h at concentrations three times higher than the IC₅₀ values of the inhibitors. The two equal parts of the same parasite culture incubated with chloroquine (0.8 µM) and DMSO were considered as positive and negative controls, respectively. Cultures were centrifuged at 894 g for 5 min and RBC pellet was treated with ice-cold 0.05% saponin in the PBS for 5 min to lyse the erythrocytes. The lysate was further centrifuged at 12 096 g for 5 min at 4 °C. In the next step, removal of the residual Hb was performed by washing the pellet twice with PBS, and the parasites were subsequently recovered by centrifugation. The parasite pellet was resuspended in 100 µL SDS/PAGE sample buffer, boiled for 10 min, and centrifuged at 27 216 g for 15 min at room temperature. Supernatants corresponding to $\sim 1.5 \times 10^7$ parasites were loaded on 15% SDS/PAGE.

Cytotoxicity assay

To check the effect of inhibitors (KNI-10743 and KNI-10333) on human cells, MTT assay was performed as previously described [63]. Briefly, HFF were incubated with different concentrations of inhibitors (1–25 µM) to measure the cytotoxicity. MTT was then added to cells and incubated at 37 °C for 4 h in dark, followed by an incubation with dimethylformamide overnight before measuring the absorbance using colorimetry. The cells treated with cisplatin (20 µM) and DMSO solvent were considered as positive and negative controls, respectively. Cell morphology was evaluated by inverted light microscopy.

Acknowledgements

We thank the EMBL staff Hassan Belrhali and Babu A. Manjasetty for providing support on the beamline and EMBL-DBT for providing access to the BM14 beamline at the ESRF. The 'Protein Crystallography Facility' at IIT Bombay is also acknowledged. VM thanks Department of Biotechnology (DBT), Ministry of Science and Technology, India, for PhD fellowship. IR acknowledges the PhD fellowship from the University Grant Commission (UGC). The work was supported by the Ramalingaswami Re-entry Fellowship (DBT), a research seed grant from IRCC, IIT Bombay to Prasenjit Bhaumik and by the Intramural Research Program of the NIH, National Cancer Institute, Center for Cancer Research. KH acknowledges the support from the Takeda Science Foundation. The financial support of the Natural Sciences and Engineering Research Council of Canada (HX and RYY) is also gratefully acknowledged. The authors also thank Nicholas Grant for reviewing the manuscript.

Conflict of interest

The authors declare no competing financial interests.

Authors' contributions

VM and IR have contributed equally. VM, IR, and PB conceived the idea and coordinated the study. VM and IR prepared the proteins and undertook the purification and crystallographic experiments under the supervision of PB. The structures were solved and structural analysis was done by VM and IR with input from PB, AG, and AW. The kinetics experiments were performed by VM with assistance from IR and suggestions from HX and RYY under the supervision of PB. The antiparasitic assay was performed by AA with an advice from SP. The cytotoxicity assay was done by LKS under the supervision of SS. The inhibitors were synthesized by KH and YK. The paper was jointly written by VM, IR, and PB with inputs from the remaining authors.

References

- White NJ, Pukrittayakamee S, Hien TT, Faiz MA, Mokuolu OA & Dondorp AM (2014) Malaria. *Lancet* **383**, 723–735.
- WHO (World Health Organisation) (2016) World malaria report 2016.
- Hanboonkunupakarn B & White NJ (2016) The threat of antimalarial drug resistance. *Trop Dis Travel Med Vaccines* **2**, 10.
- Müller IB & Hyde JE (2010) Antimalarial drugs: modes of action and mechanisms of parasite resistance. *Future Microbiol* **5**, 1857–1873.
- Ball EG, McKee RW, Anfinson CB, Cruz WO & Geiman QM (1948) Studies on malarial parasites; chemical and metabolic changes during growth and multiplication *in vivo* and *in vitro*. *J Biol Chem* **175**, 547–571.
- Olliaro PL & Goldberg DE (1995) The *Plasmodium* digestive vacuole: metabolic headquarters and choice drug target. *Parasitol Today* **11**, 294–297.
- Coombs GH, Goldberg DE, Klemba M, Berry C, Kay J & Mottram JC (2001) Aspartic proteases of *Plasmodium falciparum* and other parasitic protozoa as drug targets. *Trends Parasitol* **17**, 532–537.
- Francis SE, Sullivan DJJ & Goldberg DE (1997) Hemoglobin metabolism in the malaria parasite *Plasmodium falciparum*. *Annu Rev Microbiol* **51**, 97–123.
- Banerjee R, Liu J, Beatty W, Pelosof L, Klemba M & Goldberg DE (2002) Four plasmepsins are active in the *Plasmodium falciparum* food vacuole, including a protease with an active-site histidine. *Proc Natl Acad Sci USA* **99**, 990–995.
- Omara-Opyene AL, Moura PA, Sulsona CR, Bonilla JA, Yowell CA, Fujioka H, Fidock DA & Dame JB (2004) Genetic disruption of the *Plasmodium falciparum* digestive vacuole plasmepsins demonstrates their functional redundancy. *J Biol Chem* **279**, 54088–54096.
- Liu J, Gluzman IY, Drew ME & Goldberg DE (2005) The role of *Plasmodium falciparum* food vacuole plasmepsins. *J Biol Chem* **280**, 1432–1437.
- Ersmark K, Samuelsson B & Hallberg A (2006) Plasmepsins as potential targets for new antimalarial therapy. *Med Res Rev* **26**, 626–666.
- Bjelic S, Nervall M, Gutiérrez-de-Terán H, Ersmark K, Hallberg A & Åqvist J (2007) Computational inhibitor design against malaria plasmepsins. *Cell Mol Life Sci* **64**, 2285–2305.
- Pons T, Gil LA, Valiente PA & Pascutti PG (2011) Computational perspectives into plasmepsins structure-function relationship: implications to inhibitors design. *J Trop Med* **2011**, 657483.
- Meyers JM & Goldberg DE (2012) Recent advances in plasmepsin medicinal chemistry and implications for future antimalarial drug discovery efforts. *Curr Top Med Chem* **12**, 445–455.
- Dan N & Bhakat S (2015) New paradigm of an old target: an update on structural biology and current progress in drug design towards plasmepsin II. *Eur J Med Chem* **95**, 324–348.
- Nezami A, Kimura T, Hidaka K, Kiso A, Liu J, Kiso Y, Goldberg DE & Freire E (2003) High-affinity inhibition of a family of *Plasmodium falciparum* proteases by a designed adaptive inhibitor. *Biochemistry* **42**, 8459–8464.

- 18 Rasina D, Otkovs M, Leitans J, Recacha R, Borysov OV, Kanepe-Lapsa I, Domranceva I, Pantelejevs T, Tars K, Blackman MJ *et al.* (2016) Fragment-based discovery of 2-Aminoquinazolin-4(3H)-ones as novel class nonpeptidomimetic inhibitors of the plasmepsins I, II, and IV. *J Med Chem* **59**, 374–387.
- 19 Huizing AP, Mondal M & Hirsch AKH (2015) Fighting malaria: structure-guided discovery of nonpeptidomimetic plasmepsin inhibitors. *J Med Chem* **58**, 5151–5163.
- 20 Recacha R, Leitans J, Akopjana I, Aprupe L, Trapencieris P, Jaudzems K, Jirgensons A & Tars K (2015) Structures of plasmepsin II from *Plasmodium falciparum* in complex with two hydroxyethylamine-based inhibitors. *Acta Crystallogr F Struct Biol Commun* **71**, 1531–1539.
- 21 Bhaumik P, Gustchina A & Wlodawer A (2012) Structural studies of vacuolar plasmepsins. *Biochim Biophys Acta* **1824**, 207–223.
- 22 Nezami A, Luque I, Kimura T, Kiso Y & Freire E (2002) Identification and characterization of allophenylnorstatine-based inhibitors of plasmepsin II, an antimalarial target. *Biochemistry* **41**, 2273–2280.
- 23 Nezami A & Freire E (2002) The integration of genomic and structural information in the development of high affinity plasmepsin inhibitors. *Int J Parasitol* **32**, 1669–1676.
- 24 Hidaka K, Kimura T, Tsuchiya Y, Kamiya M, Ruben AJ, Freire E, Hayashi Y & Kiso Y (2007) Additional interaction of allophenylnorstatine-containing tripeptidomimetics with malarial aspartic protease plasmepsin II. *Bioorganic Med Chem Lett* **17**, 3048–3052.
- 25 Miura T, Hidaka K, Uemura T, Kashimoto K, Hori Y, Kawasaki Y, Ruben AJ, Freire E, Kimura T & Kiso Y (2010) Improvement of both plasmepsin inhibitory activity and antimalarial activity by 2-aminoethylamino substitution. *Bioorganic Med Chem Lett* **20**, 4836–4839.
- 26 Goldberg DE, Slater AF, Beavis R, Chait B, Cerami A & Henderson GB (1991) Hemoglobin degradation in the human malaria pathogen *Plasmodium falciparum*: a catabolic pathway initiated by a specific aspartic protease. *J Exp Med* **173**, 961–969.
- 27 Clemente JC, Govindasamy L, Madabushi A, Fisher SZ, Moose RE, Yowell CA, Hidaka K, Kimura T, Hayashi Y, Kiso Y *et al.* (2006) Structure of the aspartic protease plasmepsin 4 from the malarial parasite *Plasmodium malariae* bound to an allophenylnorstatine-based inhibitor. *Acta Crystallogr D Biol Crystallogr* **62**, 246–252.
- 28 Bhaumik P, Xiao H, Parr CL, Kiso Y, Gustchina A, Yada RY & Wlodawer A (2009) Crystal structures of the histo-aspartic protease (HAP) from *Plasmodium falciparum*. *J Mol Biol* **388**, 520–540.
- 29 Bhaumik P, Horimoto Y, Xiao H, Miura T, Hidaka K, Kiso Y, Wlodawer A, Yada RY & Gustchina A (2011) Crystal structures of the free and inhibited forms of plasmepsin I (PMI) from *Plasmodium falciparum*. *J Struct Biol* **175**, 73–84.
- 30 Boddey JA, Hodder AN, Günther S, Gilson PR, Patsiouras H, Kapp EA, Pearce JA, de Koning-Ward TF, Simpson RJ, Crabb BS *et al.* (2010) An aspartyl protease directs malaria effector proteins to the host cell. *Nature* **463**, 627–631.
- 31 Mastan BS, Kumari A, Gupta D, Mishra S & Kumar KA (2014) Gene disruption reveals a dispensable role for Plasmepsin VII in the *Plasmodium berghei* life cycle. *Mol Biochem Parasitol* **195**, 10–13.
- 32 Li F, Bounkeua V, Pettersen K & Vinetz JM (2016) *Plasmodium falciparum* ookinete expression of plasmepsin VII and plasmepsin X. *Malar J* **15**, 111.
- 33 Mastan BS, Narwal SK, Dey S, Kumar KA & Mishra S (2017) *Plasmodium berghei* plasmepsin VIII is essential for sporozoite gliding motility. *Int J Parasitol* **47**, 239–245.
- 34 Xiao H, Bryksa BC, Bhaumik P, Gustchina A, Kiso Y, Yao SQ, Wlodawer A & Yada RY (2014) The zymogen of plasmepsin V from *Plasmodium falciparum* is enzymatically active. *Mol Biochem Parasitol* **197**, 56–63.
- 35 Bedi RK, Patel C, Mishra V, Xiao H, Yada RY & Bhaumik P (2016) Understanding the structural basis of substrate recognition by *Plasmodium falciparum* plasmepsin V to aid in the design of potent inhibitors. *Sci Rep* **6**, 31420.
- 36 Davies DR (1990) The structure and function of the aspartic proteinases. *Annu Rev Biophys Biophys Chem* **19**, 189–215.
- 37 Coates L, Erskine PT, Crump MP, Wood SP & Cooper JB (2002) Five atomic resolution structures of endothiapepsin inhibitor complexes: implications for the aspartic proteinase mechanism. *J Mol Biol* **318**, 1405–1415.
- 38 Robbins AH, Dunn BM, Agbandje-Mckenna M & McKenna R (2009) Crystallographic evidence for noncoplanar catalytic aspartic acids in plasmepsin II resides in the Protein Data Bank. *Acta Crystallogr D Biol Crystallogr* **65**, 294–296.
- 39 Wallace AC, Laskowski RA & Thornton JM (1995) LIGPLOT: a program to generate schematic diagrams of protein-ligand interactions. *Protein Eng Des Sel* **8**, 127–134.
- 40 Kiso Y (1996) Design and synthesis of substrate-based peptidomimetic human immunodeficiency virus protease inhibitors containing the hydroxymethylcarbonyl isostere. *Biopolymers* **40**, 235–244.
- 41 Prade L, Jones AF, Boss C, Richard-Bildstein S, Meyer S, Binkert C & Bur D (2005) X-ray structure of plasmepsin II complexed with a potent achiral inhibitor. *J Biol Chem* **280**, 23837–23843.

- 42 Parr-Vasquez CL & Yada RY (2010) Functional chimera of porcine pepsin prosegment and *Plasmodium falciparum* plasmepsin II. *Protein Eng Des Sel* **23**, 19–26.
- 43 Xiao H, Tanaka T, Ogawa M & Yada RY (2007) Expression and enzymatic characterization of the soluble recombinant plasmepsin I from *Plasmodium falciparum*. *Protein Eng Des Sel* **20**, 625–633.
- 44 Bradford MM (1976) A rapid and sensitive method for the quantitation of microgram quantities of protein utilizing the principle of protein-dye binding. *Anal Biochem* **72**, 248–254.
- 45 Istvan ES & Goldberg DE (2005) Distal substrate interactions enhance plasmepsin activity. *J Biol Chem* **280**, 6890–6896.
- 46 Windsor IW & Raines RT (2015) Fluorogenic assay for inhibitors of HIV-1 protease with sub-picomolar affinity. *Sci Rep* **5**, 11286.
- 47 Morrison JF (1969) Kinetics of the reversible inhibition of enzyme-catalysed reactions by tight-binding inhibitors. *Biochim Biophys Acta* **185**, 269–286.
- 48 Kabsch W (2010) XDS. *Acta Crystallogr D Biol Crystallogr* **66**, 125–132.
- 49 Winn MD, Ballard CC, Cowtan KD, Dodson EJ, Emsley P, Evans PR, Keegan RM, Krissinel EB, Leslie AGW, McCoy A *et al.* (2011) Overview of the CCP 4 suite and current developments. *Acta Crystallogr D Biol Crystallogr* **67**, 235–242.
- 50 Matthews BW (1968) Solvent content of protein crystals. *J Mol Biol* **33**, 491–497.
- 51 McCoy AJ, Grosse-Kunstleve RW, Adams PD, Winn MD, Storoni LC & Read RJ (2007) Phaser crystallographic software. *J Appl Crystallogr* **40**, 658–674.
- 52 Murshudov GN, Vagin AA & Dodson EJ (1997) Refinement of macromolecular structures by the maximum-likelihood method. *Acta Crystallogr D Biol Crystallogr* **53**, 240–255.
- 53 Moriarty NW, Grosse-Kunstleve RW & Adams PD (2009) Electronic ligand builder and optimization workbench (eLBOW): a tool for ligand coordinate and restraint generation. *Acta Crystallogr D Biol Crystallogr* **65**, 1074–1080.
- 54 Afonine PV, Grosse-Kunstleve RW, Echols N, Headd JJ, Moriarty NW, Mustyakimov M, Terwilliger TC, Urzhumtsev A, Zwart PH & Adams PD (2012) Towards automated crystallographic structure refinement with *phenix.refine*. *Acta Crystallogr D Biol Crystallogr* **68**, 352–367.
- 55 Emsley P & Cowtan K (2004) Coot: model-building tools for molecular graphics. *Acta Crystallogr D Biol Crystallogr* **60**, 2126–2132.
- 56 Painter J & Merritt EA (2006) Optimal description of a protein structure in terms of multiple groups undergoing TLS motion. *Acta Crystallogr D Biol Crystallogr* **62**, 439–450.
- 57 Davis IW, Murray LW, Richardson JS & Richardson DC (2004) MOLPROBITY: structure validation and all-atom contact analysis for nucleic acids and their complexes. *Nucleic Acids Res* **32**, W615–W619.
- 58 Zolg JW, MacLeod AJ, Dickson IH & Scaife JG (1982) *Plasmodium falciparum*: modifications of the *in vitro* culture conditions improving parasitic yields. *J Parasitol* **68**, 1072–1080.
- 59 Cranmer SL, Magowan C, Liang J, Coppel RL & Cooke BM (1997) An alternative to serum for cultivation of *Plasmodium falciparum* *in vitro*. *Trans R Soc Trop Med Hyg* **91**, 363–365.
- 60 Lambros C & Vanderberg JP (1979) Synchronization of *Plasmodium falciparum* erythrocytic stages in culture. *J Parasitol* **65**, 418–420.
- 61 Prasad R, Atul , Kolla VK, Legac J, Singhal N, Navale R, Rosenthal PJ & Sijwali PS (2013) Blocking *Plasmodium falciparum* development via dual inhibition of hemoglobin degradation and the ubiquitin proteasome system by MG132. *PLoS ONE* **8**, e73530.
- 62 Zhang Y (1987) Inhibition of hemoglobin degradation in *Plasmodium falciparum* by chloroquine and ammonium chloride. *Exp Parasitol* **64**, 322–327.
- 63 Fotakis G & Timbrell JA (2006) *In vitro* cytotoxicity assays: comparison of LDH, neutral red, MTT and protein assay in hepatoma cell lines following exposure to cadmium chloride. *Toxicol Lett* **160**, 171–177.